International Journal of Innovative Research and Scientific Studies, 8(6) 2025, pages: 1002-1015

IJIRSS
International Journal of Innovative Research & Scientific Studies

ISSN: 2617-6548

URL: www.ijirss.com

Spatiotemporal coupling of correlation fractal dimension and b-value in seismic zones of Taiwan: Statistical trends, regional variations, and physical implications

Hu Huang[1], Boi-Yee Liao[1*]

[1]*Institute of Engineering Technology Management, International College, Krirk University, 3 Ram Inthra Rd, Anusawari, Bang Khen, Bangkok 10220, Thailand.*

Corresponding author: Boi-Yee Liao (*Email: y5708211@ms18.hinet.net*)

Abstract

This study investigates the spatiotemporal relationship between the correlation fractal dimension (Dc) and the Gutenberg–Richter b-value across 27 seismic zones in Taiwan, using earthquake catalog data from 1973 to 2023. Temporal evolution curves reveal diverse Dc trends, with several eastern and central zones (e.g., S04, S14A, S06) showing pronounced long-term decreases, potentially reflecting stress concentration and fault segmentation effects. Spatial mapping of earthquake epicenters and event statistics highlights strong heterogeneity in seismic productivity. Regression analyses indicate significant positive Dc–b correlations in selected zones, with Pearson's R^2 exceeding 0.8 in S05B, S06, and S17A, implying consistent scaling behavior between magnitude–frequency distributions and spatial clustering. Fixed-window versus cumulative-window b-value comparisons reveal that Δb variations are most pronounced in tectonically active zones, coinciding with higher Kendall and Pearson correlation coefficients between Dc and b-values. These results demonstrate that the coupled evolution of Dc and b-values provides a sensitive indicator of seismogenic state changes, particularly in regions with persistent stress loading. The proposed multi-parameter approach offers new potential for seismic hazard assessment by integrating spatial fractal analysis with temporal magnitude–frequency variations, thereby enhancing the understanding of regional earthquake preparation processes in Taiwan's complex tectonic environment.

Keywords: B-Value, Correlation fractal dimension (Dc), Kendall rank correlation coefficient, Mann-Kendall test.

DOI: 10.53894/ijirss.v8i6.9780
Funding: This study received no specific financial support. The APC was funded by Krirk University, Thailand.
History: Received: 25 July 2025 / **Revised:** 27 August 2025 / **Accepted:** 29 August 2025 / **Published:** 10 September 2025

Competing Interests: The authors declare that they have no competing interests.
Authors' Contributions: Both authors contributed equally to the conception and design of the study. Both authors have read and agreed to the published version of the manuscript.
Transparency: The authors confirm that the manuscript is an honest, accurate, and transparent account of the study; that no vital features of the study have been omitted; and that any discrepancies from the study as planned have been explained. This study followed all ethical practices during writing.
Publisher: Innovative Research Publishing

1. Introduction

The spatiotemporal evolution of earthquake statistical parameters, particularly the Gutenberg–Richter frequency–magnitude b-value and the correlation fractal dimension (Dc) has long been investigated as a means of characterizing fault stress state, rupture heterogeneity, and aftershock clustering [1-3]. The b-value, which quantifies the relative proportion of

small to large earthquakes, is widely regarded as inversely correlated with differential stress in the brittle crust [4]. In parallel, the correlation dimension Dc describes the spatial clustering of earthquake hypocenters or epicenters, with higher values reflecting more complex and heterogeneous fault-zone geometries [5, 6].

Recent evidence indicates that b and Dc are not merely independent descriptors but may exhibit coupled behavior governed by shared physical mechanisms such as fault segmentation, stress accumulation, and rupture dynamics. For example, Wyss et al. [7] reported a positive correlation between b and Dc along the Parkfield segment of the San Andreas Fault, distinguishing creeping from locked sections according to their position on the b–Dc trend. Similar patterns were observed in western Anatolia, where low b and high Dc values marked asperities and stress concentration zones, while high b–Dc values characterized diffuse seismicity under lower stress conditions Bayrak et al. [8]. Helmstetter et al. [9] further demonstrated that when b > D/2b, small earthquakes may dominate stress redistribution and triggering, underscoring the importance of jointly analyzing these parameters.

Comparable relationships have been documented worldwide. In the central Himalaya, the 2015 Gorkha and Dolakha earthquakes were accompanied by co-variations in b, Dc, and the p-value of aftershock decay, with low b–high Dc regions corresponding to zones of high Coseismic slip [10]. The 2023 Türkiye doublet earthquakes likewise exhibited spatial heterogeneity in b and Dc that mirrored rupture geometry and aftershock productivity [11]. In Iran, Firoozfar and Ansari [12] identified tectonic-domain-dependent deviations from Aki's scaling, while Setyawan and Sapiie [13] observed multiple D_2–D_0 scaling regimes in Sumatra associated with complex rupture processes. Aftershock analyses of the 1999 Chamoli earthquake also revealed spatial variations in b and D_c near major fault boundaries [14], and similar behavior was reported in the Koyna–Warna reservoir region, where temporal Dc changes correlated with pore pressure variations and stress-induced b-value fluctuations [15].

More recently, three-dimensional mapping of b and Dc has enriched seismic hazard interpretation. Mandal et al. [16] demonstrated vertical and lateral heterogeneity in the Uttarakhand Himalaya, where low B–high Dc zones often coincided with locked asperities. Expanding this approach, Mandal et al. [17] incorporated 3D b–Dc modeling into regional hazard assessments in Ladakh and neighboring Himalayan regions. Their results emphasized that low b–low Dc combinations signal elevated seismic risk, whereas high b–high Dc values denote fractured or creeping segments, thus supporting the integration of b–Dc co-variations into probabilistic hazard frameworks.

Despite these advances, critical gaps remain. First, most studies still treat b-value and Dc independently, leaving the physical basis of their co-evolution under varying stress, thermal, and fluid regimes insufficiently resolved. Second, the depth dependence of b–Dc relationships is seldom addressed systematically, even though deep crustal processes likely influence seismogenesis in thick fault zones such as Taiwan and the Himalayas. Third, although low b–high Dc zones are often interpreted as asperities, their long-term persistence or recurrence has rarely been evaluated using homogeneous earthquake catalogs. Finally, the incorporation of b–Dc relationships into time-dependent probabilistic seismic hazard assessment (PSHA) remains limited, despite their potential to enhance both short-term forecasting and long-term hazard estimation.

To address these issues, this study examines the coupled spatiotemporal evolution of b and Dc across 28 seismic zones in Taiwan over 50 years (1973–2023), using a unified earthquake catalog. Both fixed and cumulative 5-year windows are employed to capture multi-scale variations, with correlations assessed using Pearson and Kendall statistics. Dc is estimated via three-dimensional two-point correlation integrals, and b-values are calculated using the maximum likelihood method. By comparing patterns across tectonic domains, including accretionary wedges, fold-thrust belts, and strike-slip corridors, this study evaluates whether b–Dc relationships reflect fundamental physical processes and explores their potential for improving seismic hazard modeling in complex crustal environments such as Taiwan.

2. Methodology

2.1. b-value Estimation

For each window, given magnitudes Mj≥Mc, the b-value is estimated via the Woessner and Wiemer [18] maximum likelihood estimator:

$$b = \frac{\log_{10} e}{\bar{M} - (M_c - \frac{\Delta M}{2})} \quad (1)$$

where $\bar{M}$ is the mean magnitude, and ΔM is the magnitude bin size (e.g., 0.1). The standard deviation is

$$\sigma_b \approx \frac{b}{\sqrt{N}} \quad (2)$$

where N represents the number of events used to calculate the b-value, specifically the earthquakes that satisfy the condition M≥Mc. We report a 95% confidence interval.

$$CI_{95\%}(b) = b \pm 1.96\sigma_b \ (3)$$

2.2. Correlation Fractal Dimension Dc

The correlation dimension is utilized to compute the Dc values, which are described by Wiemer and Wyss [19] as follows:

$$D_c = \lim_{\varepsilon \to 0} \frac{\log C(\varepsilon)}{\log \varepsilon} \ (4)$$

$$C(\varepsilon) = \frac{1}{N(N-1)} \sum_{i \neq j} H(\varepsilon - |x_i - x_j|) \ (5)$$

where H is the Heaviside step function. The summation of H represents the count of distances between pairs of (x_i, x_j) smaller than ε. If the distribution of epicenters satisfies a fractal structure, the correlation between C(ε) and D_c is expressed as

$$C(\varepsilon) \sim \varepsilon^{D_c} \quad (6)$$

The fractal dimension Dc of the spatial distribution of earthquakes is estimated using this relationship.

2.3. Kendall Rank Correlation Coefficient Analysis

To quantify the monotonic relationship between the temporal evolution of the b-value and the correlation fractal dimension (Dc) across seismic zones, we employed the Kendall rank correlation coefficient (Kendall's τ). This non-parametric statistic is particularly well-suited for ordinal data, small samples, or variables that do not necessarily follow a linear or normal distribution. For each seismic zone, time series of b-values and Dc-values were extracted using fixed 5-year windows from 1973 to 2023. Let (x_i, y_i) denote paired values of b and Dc at time i. Kendall's τ is computed based on the number of concordant (C) and discordant (D) pairs as follows:

$$\tau = \frac{C-D}{\frac{1}{2}n(n-1)} \quad (7)$$

A pair (x_i,y_i) and (x_j,y_j) is concordant if $(x_i-x_j)(y_i-y_j)>0$, discordant if $(x_i-x_j)(y_i-y_j)<0$, and tied if either $x_i=x_j$ or $y_i=y_j$, in which case the pair is excluded from the computation. The resulting τ values range from –1 (perfect inverse relationship) to +1 (perfect direct relationship), with τ = 0 indicating no association. This coefficient provides a robust measure of co-evolutionary trends between seismic parameters without assuming specific distributional forms. Significant positive or negative τ values were interpreted as indicating zones with synchronous or opposing temporal trends in b-value and Dc-value, respectively, potentially reflecting different seismotectonic processes.

2.4. Ordinary Least Squares (OLS) linear regression.

In this study, the relationship between the Gutenberg–Richter b-value and the correlation fractal dimension (Dc) was examined using Ordinary Least Squares (OLS) linear regression. The model assumes a linear functional form:

$$Dc_i = \beta 0 + \beta 1 * b_i + \varepsilon_i \quad (8)$$

where Dc_i is the observed fractal dimension for the i-th time window in a given seismic zone, b_i is the corresponding b-value, β0 is the intercept, β1 is the slope representing the degree of b–Dc coupling, ε_i is the residual error term. The OLS method determines β0 and β1 by minimizing the Residual Sum of Squares (RSS):

$$RSS(\beta 0, \beta 1) = \sum [D_{c_i} - (\beta 0 + \beta 1 * b_i)]^2 \quad (9)$$

The closed-form solutions are

$$\widehat{\beta 1} = \frac{\sum (b_i - \bar{b})(D_{c_i} - \overline{D_c})}{\sum (b_i - \bar{b})^2} \quad (10)$$

$$\widehat{\beta 0} = \overline{D_c} - \widehat{\beta 1} * \bar{b} \quad (11)$$

where $\bar{b}$ and $\overline{D_c}$ are the sample means of b and Dc.

The model's explanatory power is quantified by the coefficient of determination (R^2):

$$R^2 = 1 - \frac{\sum [D_{c_i} - (\widehat{\beta 0} + \widehat{\beta 1})]^2}{\sum (D_{c_i} - \overline{D_c})^2} (12)$$

An R^2 value close to 1 indicates a strong linear association. The significance of β1 was assessed using a t-test:

$$t = \frac{\widehat{\beta 1}}{SE(\widehat{\beta 1})} (13)$$

where

$$SE(\widehat{\beta 1}) = \sqrt{\frac{\sigma^2}{\sum (b_i - \bar{b})^2}} \quad (14)$$

$$\sigma^2 = RSS / (n - 2) \quad (15)$$

The p-value determines if β1 is significantly different from zero. A 95% confidence interval for the regression line was calculated as:

$$\widehat{D_c}(b0) \pm t_{\alpha/2, n-1} * SE_{fit}(b0) \quad (16)$$

$$SE_{fit}(b0) = \sigma * \sqrt{\frac{1}{n} + \frac{(b0 - \bar{b})^2}{\sum (b_i - \bar{b})^2}} \quad (17)$$

Parameter $t_{\alpha/2, n-1}$ indicates the critical value of a two-tailed t-distribution at significance level α with n−1 degrees of freedom. This CI represents the uncertainty in the mean predicted Dc for a given b=b0.

3. Results and Discussions

3.1. Classification of b-Value Variation Patterns

In this study, we analyzed the seismic activity of Taiwan by first dividing the island into 28 seismic zones (S01–S21) following Cheng et al. [20]. The earthquake catalog spanning 1973–2023 was compiled for analysis (Figures 1 and 2).

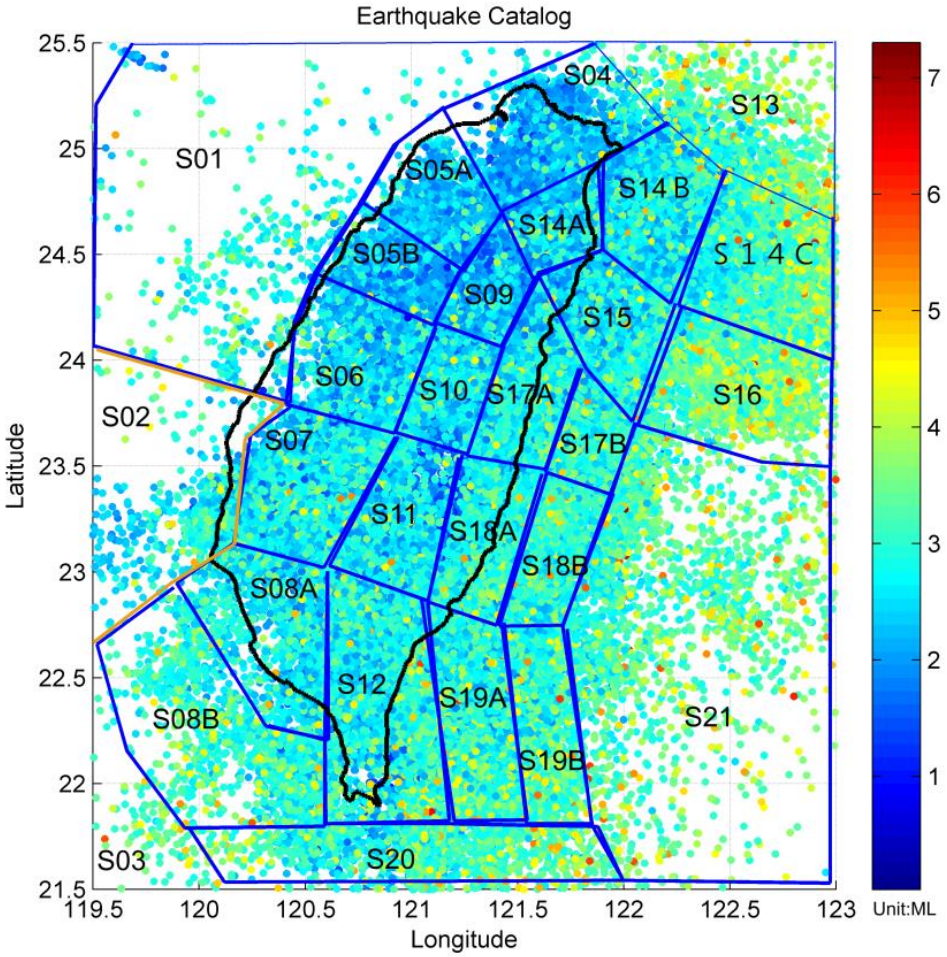

Figure 1.
Seismic zoning of Taiwan and the earthquake catalog used in this study. The island is divided into 28 seismic zones (S01–S21) following Cheng et al. [20]. Earthquake epicenters from the 1973–2023 catalog are plotted, illustrating the spatial distribution of seismicity across the zones. The declustered catalog, obtained by applying the spatiotemporal method of Gardner and Knopoff [21], serves as the basis for subsequent b-value analyses, including both continuous and 5-year interval evaluations.

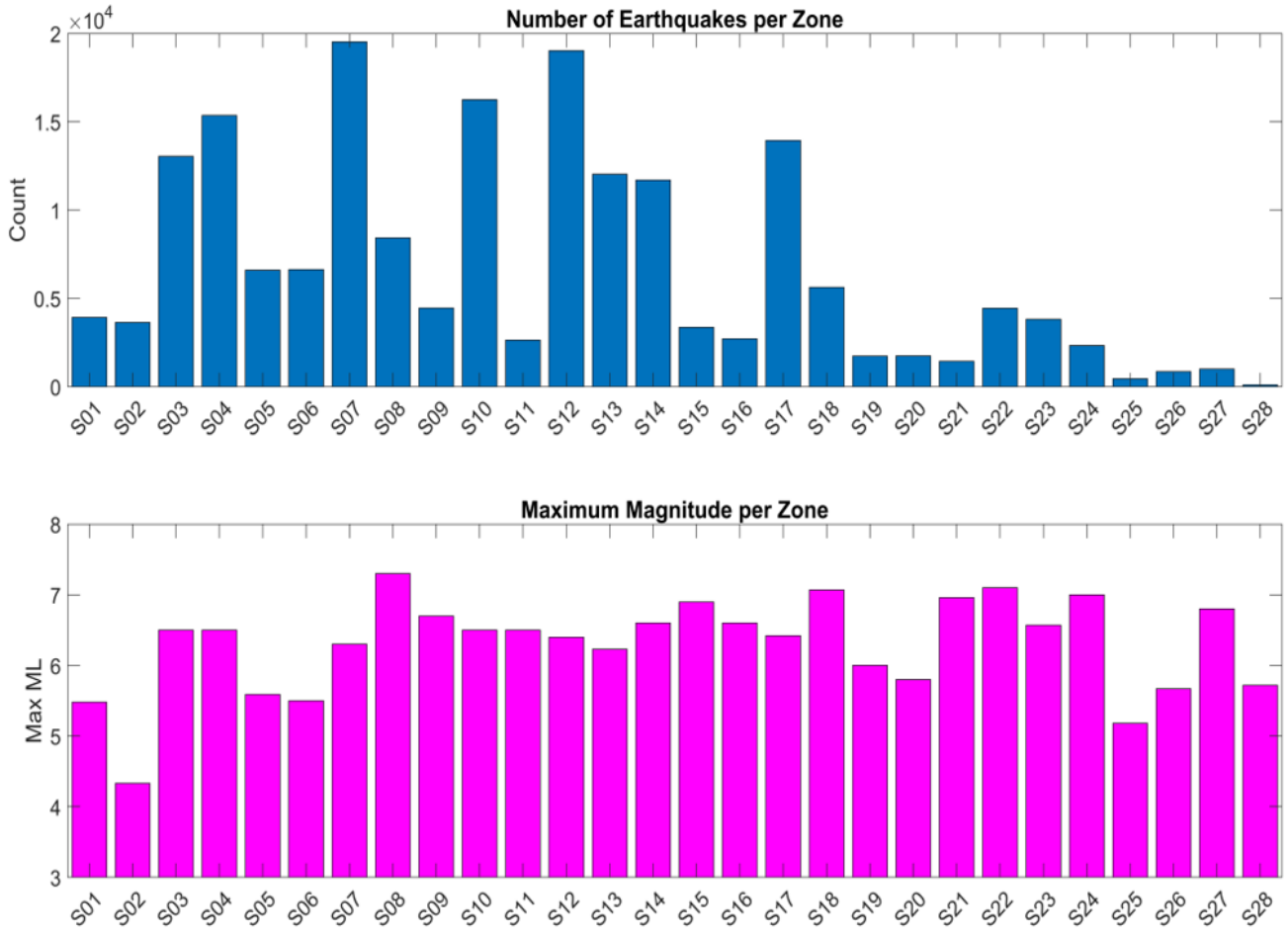

Figure 2.
Seismic activity statistics across the 28 defined zones in Taiwan. (a) Number of earthquakes per zone from 1973 to 2023, based on the declustered catalog. (b) The maximum local magnitude (ML) observed in each zone during the same period. The results highlight significant variability in both earthquake occurrence and maximum magnitude across different tectonic regions.

To reduce the influence of aftershocks and foreshocks, we employed a spatiotemporal declustering method [21]. Subsequently, both continuous b-value analysis and segmented b-value analysis with a 5-year interval were conducted for each seismic zone. Applying the equations described in section 2.1, the comparative analysis of fixed- and cumulative-window b-values across the 16 selected seismic zones is demonstrated in Figure 3 and the detailed discussions will be presented in the later sections.

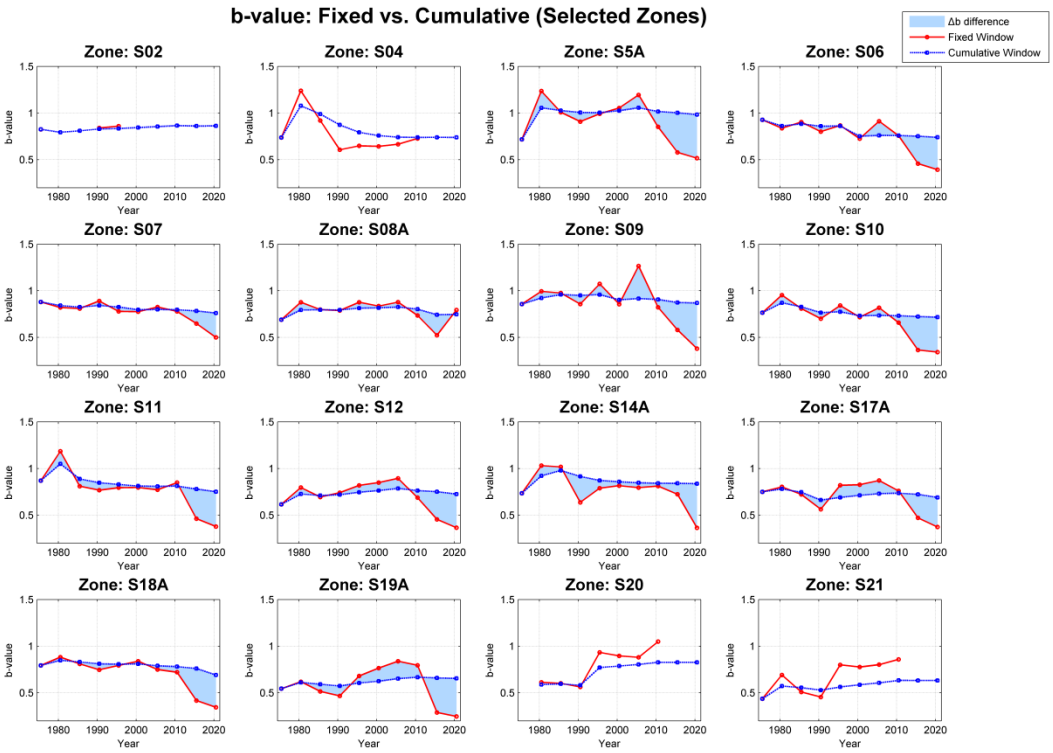

Figure 3.
Comparison of b-value evolution between fixed-window and cumulative-window methods for selected seismic zones in Taiwan. Each panel shows temporal variations of the b-value from 1973 to 2023, with the fixed-window results (red line), cumulative-window results (blue line), and their differences highlighted by the shaded area. The results reveal both stable and fluctuating b-value patterns across zones, reflecting regional heterogeneity in stress conditions and seismicity characteristics.

The comparative analysis of cumulative- and fixed-window b-values, together with their difference (Δb), provides a coherent framework for interpreting temporal variations in seismicity. The cumulative-window b-value, computed using the entire catalog up to a given time, serves as a stable long-term baseline that reflects the background stress state. In contrast, the fixed-window b-value, derived from sliding 5-year intervals, offers higher temporal resolution and is particularly sensitive to short-term perturbations such as mainshock–aftershock sequences or swarms. Their difference, Δb, quantifies the departure of short-term behavior from the long-term baseline and thus serves as a diagnostic indicator of transient stress anomalies.

The results (Fig. 3) reveal four characteristic patterns. First, long-term decreasing zones (e.g., S06, S07, S11, S18A) show consistent downward trends in both cumulative and fixed estimates, accompanied by persistently negative Δb, suggesting progressive stress accumulation and an elevated potential for larger-magnitude events. Second, short-term anomalous decreases (e.g., S05A, S09, S10, S14A) are marked by abrupt drops in fixed-window b-values that diverge from smoother cumulative trends, producing pronounced Δb anomalies indicative of transient stress perturbations. Third, fluctuating zones (e.g., S04, S11, S17A) exhibit temporary troughs in fixed-window b-values followed by recovery toward the cumulative baseline, a pattern consistent with post-seismic relaxation and Omori-type aftershock decay. Finally, relatively stable zones (e.g., S02, S08A, S12, S20) show only minor variations in both measures, yielding persistently small Δb values that reflect balanced stress regimes with limited short-term triggering potential.

Taken together, these findings underscore the complementarity of the two approaches: fixed-window b-values provide sensitivity to rapid anomalies, while cumulative-window values define a robust long-term reference. The Δb parameter operationalizes their integration by highlighting the magnitude and timing of deviations between the two, thereby enhancing the capacity to distinguish stress-accumulating regions from stress-dissipating ones. This combined perspective not only refines the interpretation of seismicity evolution but also offers a practical means of incorporating non-stationary stress information into probabilistic seismic hazard assessments.

3.2. Mann–Kendall Trend Analysis of Cumulative B-Values

To further quantify temporal variations in seismicity, a Mann–Kendall (M–K) trend test was applied to the cumulative b-value time series in each seismic zone. The statistical criteria are interpreted as follows: a p-value < 0.05 indicates that the trend is statistically significant and reliable; τ (shown in equation 7) > 0 reflects an increasing b-value (suggesting enhanced small-magnitude activity and stress release), whereas $\tau < 0$ denotes a decreasing b-value (indicating relatively more frequent larger events and stress accumulation). The corresponding results are shown in Table 1.

Table 1.
Mann-Kendall trend analysis.

Zone	p-value	τ (tau)	Trend
S04	0.0318	–0.5556	Decreasing
S5A	0.4743	–0.2000	No trend
S14A	0.0318	–0.5556	Decreasing
S14B	0.1074	0.4222	No trend
S5B	0.0491	0.5111	Increasing
S09	0.2105	–0.3333	No trend
S15	0.3711	0.2444	No trend
S06	0.0024	–0.7778	Decreasing
S10	0.0073	–0.6889	Decreasing
S17A	0.2105	–0.3333	No trend
S17B	0.0200	0.6000	Increasing
S07	0.0013	–0.8222	Decreasing
S11	0.0007	–0.8667	Decreasing
S18A	0.0042	–0.7333	Decreasing
S18B	0.4743	–0.2000	No trend
S08A	0.4743	0.2000	No trend
S12	0.1074	0.4222	No trend
S19A	0.0073	0.6889	Increasing
S19B	0.0073	0.6889	Increasing
S08B	0.0165	0.6667	Increasing
S20	0.0017	0.8611	Increasing
S14C	0.0153	0.6222	Increasing
S16	0.0153	0.6222	Increasing
S21	0.0054	0.7111	Increasing
S01	0.0476	0.5556	Increasing
S02	0.0013	0.8222	Increasing
S13	0.0592	0.5278	No trend

The results reveal three distinct groups of zones. First, significant decreasing trends were identified in Zones S04, S14A, S06, S07, S10, S11, and S18A, all exhibiting negative τ values with high significance. Among these, Zones S07 ($\tau = -0.822$, $p = 0.0013$) and S11 ($\tau = -0.867$, $p = 0.0007$) demonstrate the strongest downward trends, suggesting reduced minor seismicity and heightened stress accumulation, thus warranting classification as high-risk regions. Similarly, S06 and S10 also exhibit marked declines, indicating their potential as critical candidates for stress evolution modeling and targeted hazard weighting in PSHA frameworks.

In contrast, a group of zones shows significant upward trends, implying enhanced seismic activity dominated by small to moderate earthquakes and effective stress release. These include S5B, S17B, S19A/B, S08B, S20, S14C, S16, S21, S01, and S02. Notably, Zone S20 exhibits the most pronounced increase ($\tau = 0.861$, $p = 0.0017$), while Zone S02 in northern Taiwan also shows strong upward activity ($\tau = 0.822$, $p = 0.0013$). These areas may serve as "stress-dissipating zones," suitable for further investigation of earthquake triggering and background stress interactions. A third group, including Zones S5A, S09, S15, S17A, S18B, S08A, S12, S13, and S14B, shows no statistically significant trend ($p > 0.05$). While some zones (e.g., S14B and S12) exhibit relatively high τ values, the lack of significance suggests that these regions may follow long-term oscillatory or non-monotonic patterns, possibly constrained by data limitations.

Overall, zones with strong trends ($|\tau| > 0.7$), such as S07, S11, S20, S02, and S06, should be prioritized as critical areas for seismic risk assessment and early warning considerations. In future probabilistic seismic hazard analysis (PSHA), τ may be incorporated as a time-dependent weighting function to facilitate non-stationary hazard modeling, thereby improving the representation of evolving seismic risk in Taiwan.

3.3. Synthesis of Window-Based and Statistical Trend Analyses

The integration of window-based observations and statistical validation provides a more comprehensive understanding of the temporal b-value evolution. The fixed-versus cumulative-window classification highlights the qualitative nature of b-value fluctuations, capturing both rapid short-term anomalies and long-term stability patterns.

In contrast, the Mann–Kendall trend test quantifies these variations by providing statistical confidence levels and directionality (τ values). Notably, several zones identified as long-term decreasing in the window-based analysis (e.g., S06, S07, S11) also emerge as statistically significant negative-trend zones in the Mann-Kendall test, reinforcing their interpretation as regions of stress accumulation and heightened seismic potential. Conversely, zones such as S20 and S02, which exhibit stable or mildly increasing behavior in the cumulative-window analysis, are statistically confirmed as strong positive-trend areas, indicative of effective stress release through frequent small events. This synthesis demonstrates that while window-based approaches are effective for visualizing temporal dynamics, the Mann-Kendall test provides essential

quantitative validation, together enabling a robust framework for incorporating b-value trends into non-stationary seismic hazard assessments.

3.4. Spatiotemporal Patterns of Dc and Their Relation to b-values

In this section, the Dc values in different seismic zones are calculated using the equations in 2.2 and the results are displayed in Figure 4.

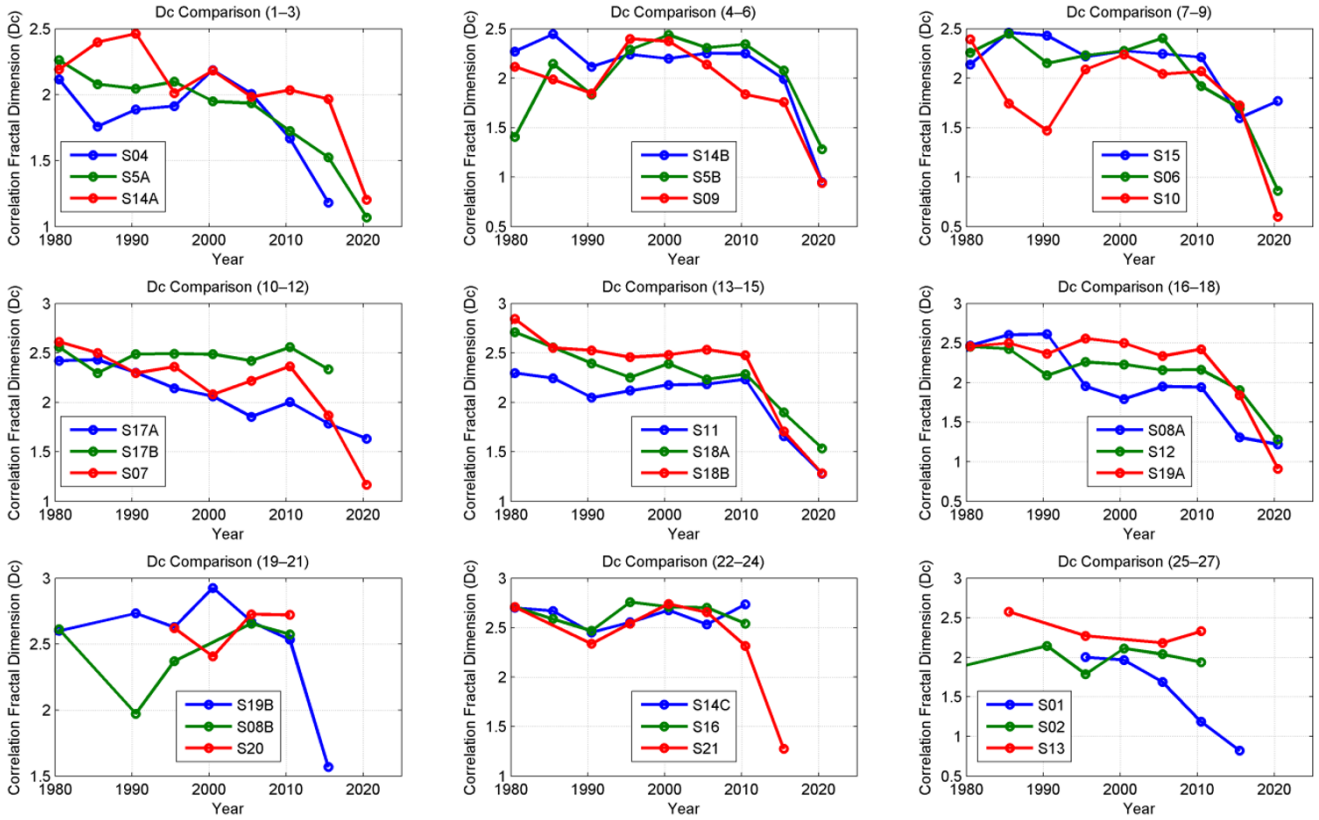

Figure 4.
Temporal evolution of the correlation fractal dimension (Dc) for 27 seismic zones in Taiwan between 1980 and 2023. Each panel shows a three-zone comparison. Most regions (e.g., S04, S07, S11, S18A, S21, S02, S13) display a clear long-term decline in Dc, indicating increasing spatial clustering of seismicity and progressive stress accumulation along active faults. In contrast, several zones (e.g., S19B, S08B, S20, S14C, S16) maintain relatively high Dc values (>2.5), reflecting dispersed seismicity and potential stress release. Notable sharp drops in Dc after 2010, observed in zones such as S07, S10, S18B, and S21, may be linked to significant regional seismic events and stress redistribution. These contrasting behaviors underscore the value of Dc as a diagnostic parameter for distinguishing stress accumulation versus release processes in different tectonic settings across Taiwan.

The temporal evolution of the correlation fractal dimension (Dc) across Taiwan's seismic zones reveals notable patterns that provide critical insights into the underlying stress regimes. A majority of zones, including S04, S07, S11, S18A, S21, S02, and S13, exhibit a pronounced long-term decline in Dc values from >2.5 to approximately 1.0, signifying a progressive transition from dispersed to increasingly clustered seismicity. This clustering reflects sustained stress accumulation and suggests the potential for future large-magnitude events in these regions. In contrast, several zones such as S19B, S08B, S20, S14C, and S16 maintain relatively high Dc values, indicative of more spatially distributed seismicity and effective stress release, which may reduce the likelihood of immediate large-scale rupture. Moreover, sharp DC reductions observed after 2010 in zones such as S07, S10, S18B, and S21 point to significant stress redistribution, likely linked to recent major seismic events. Taken together, these patterns emphasize that Dc serves as a robust diagnostic measure of spatiotemporal clustering, offering critical complementary information to b-value trends for distinguishing zones of stress accumulation from those of stress release within Taiwan's active tectonic framework.

When considered in conjunction with b-value variations, the Dc results provide a more comprehensive perspective on fault system dynamics. Zones exhibiting simultaneous decreases in both Dc and b-values, such as S07, S11, and S18A, strongly suggest stress accumulation accompanied by reduced small-magnitude seismicity and increased clustering hallmarks of heightened seismic potential. It is worth noting that an earthquake of ML 7.1 struck seismic zone S18A on 3 April 2024, followed by another significant event of ML 6.4 in seismic zone S07 on 21 January 2025. These occurrences provide strong validation of our results.

Conversely, regions where Dc remains elevated while b-values trend upward, such as S20 and S02, likely represent stress-dissipating environments characterized by abundant small events and spatially distributed rupture patterns. This complementary behavior underscores the diagnostic value of integrating b-value and Dc analyses: while b-values capture the magnitude–frequency relationship and stress sensitivity, Dc highlights the spatial organization of seismicity. Together, these dual perspectives refine our ability to distinguish between zones undergoing critical stress loading and those

functioning as energy-release domains, thereby enhancing the robustness of non-stationary seismic hazard assessments in Taiwan.

3.5. Integrated Interpretation of DC–b–value Classifications

The joint consideration of Dc and b-value trends allows for a systematic classification of Taiwan's seismic zones into four distinct categories (Table 2).

Table 2.
Integrated classification of seismic zones based on combined Dc and b-value trends.

Dc Trend	b-value Trend	Interpretation	Representative Zones	Seismotectonic Implications
Decreasing (↓)	Decreasing (↓)	High-risk accumulation zones	S07, S11, S18A	Stress build-up, reduced small-magnitude activity, strong clustering, and elevated potential for large events.
Increasing / Stable (↑/→)	Increasing (↑)	Stress-dissipating zones	S20, S02	Frequent small events, spatially distributed seismicity, and effective stress release
Decreasing (↓)	Increasing (↑)	Transitional/complex zones	(e.g., S04, S14A, S10)	Possible localized stress concentration with concurrent release; requires close monitoring
Increasing / Stable (↑/→)	Decreasing (↓)	Rare anomalous zones	Few or none identified	Potentially linked to unusual stress redistribution or catalog limitations; interpretation requires caution.

Zones exhibiting concurrent decreases in both Dc and b-values (e.g., S07, S11, S18A) represent the most critical areas, as they signal pronounced clustering alongside reduced small-magnitude activity hallmarks of stress accumulation and heightened seismic hazard. By contrast, regions with simultaneous increases in Dc and b-values, such as S20 and S02, can be interpreted as stress-dissipating zones where frequent small earthquakes help to distribute strain and mitigate the immediate likelihood of major ruptures.

Intermediate cases highlight the complexity of seismotectonic processes. For instance, zones characterized by decreasing Dc but increasing b-values (e.g., S04, S14A, S10) suggest transitional regimes where spatial clustering intensifies even as the frequency–magnitude relationship indicates energy release through smaller events. These areas may reflect localized fault interactions or short-lived stress perturbations, requiring close monitoring. Rare anomalous zones, defined by increasing Dc coupled with decreasing b-values, were scarcely observed in this study but could indicate unusual stress redistribution or catalog limitations, and thus should be treated with interpretive caution.

Overall, this integrated classification demonstrates that combining Dc with b-values yields a more robust diagnostic framework than using either parameter alone. While b-values quantify stress sensitivity through magnitude–frequency distributions, Dc captures the evolving spatial organization of seismicity. Together, they refine the ability to distinguish stress-accumulating, stress-releasing, and transitional zones, thereby providing a valuable foundation for incorporating time-dependent weighting schemes into probabilistic seismic hazard analysis and enhancing the assessment of non-stationary seismic risk in Taiwan.

3.6. Regression Analysis Between b-value and Correlation Fractal Dimension

To further quantify the relationship between earthquake magnitude distribution and spatial clustering, we performed linear regression analyses between b-value and correlation fractal dimension (Dc) across seismic zones. Figure 5 demonstrates the results of the regression relationships.

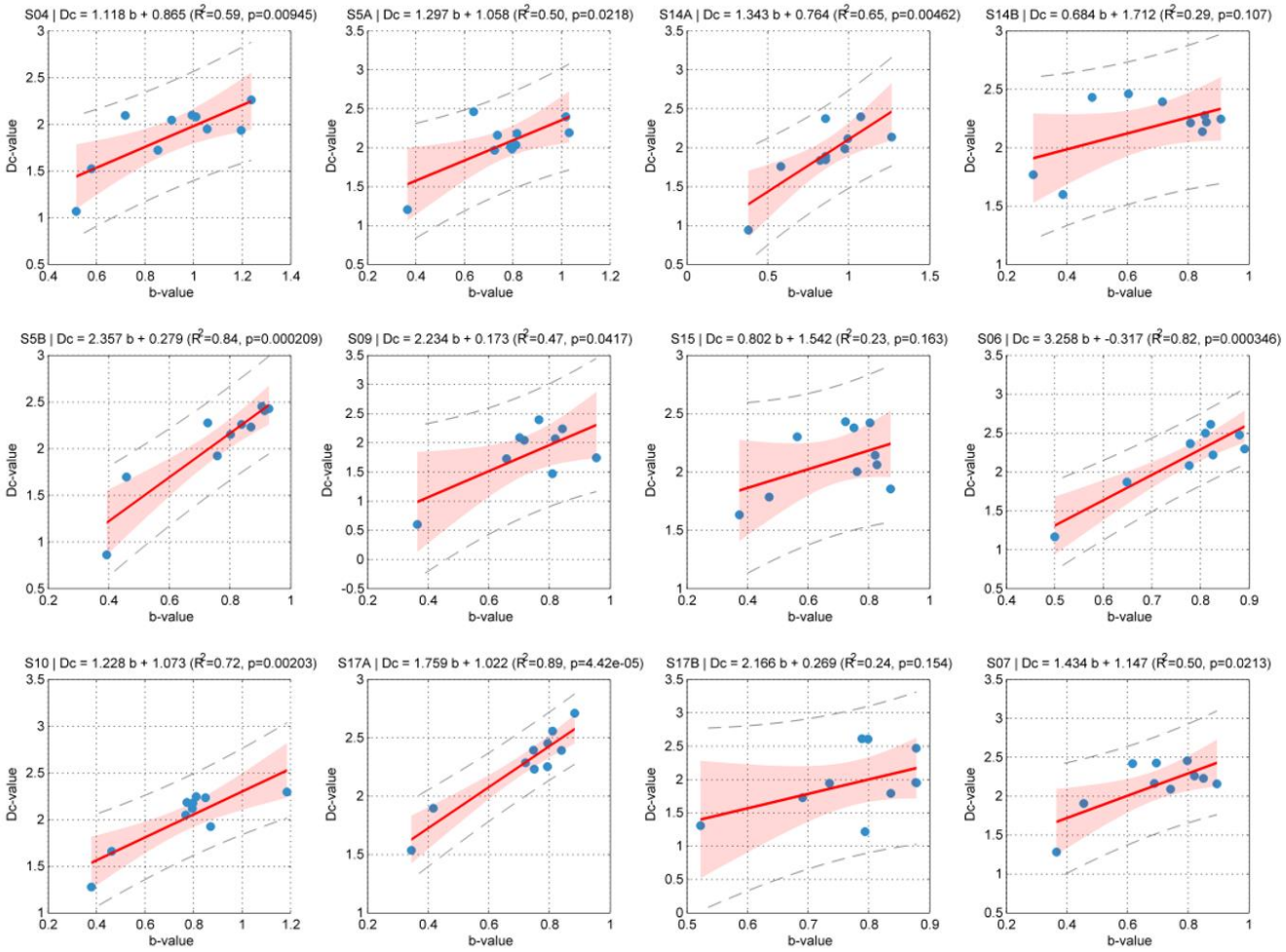

Figure 5.
Linear regression relationships between b-value and Dc-value across selected seismic zones. Each subplot presents the fitted regression line (solid red), 95% confidence interval (shaded area), and the associated regression equation, R^2 value, and p-value. Results suggest varying degrees of positive correlation across regions, with some zones (e.g., S5B, S10, S17A) exhibiting strong linear dependence, while others show weaker or statistically insignificant trends.

A systematic analysis of the linear relationship between b-value and correlation fractal dimension (Dc) across multiple seismic zones in Taiwan reveals several noteworthy patterns. In the majority of studied regions (e.g., S04, S5A, S14A, S5B, S09, S10, S17A), a statistically significant positive correlation is observed, with regression slopes ranging from approximately 0.8 to 3.25. This consistent trend suggests a coupling between earthquake frequency–magnitude characteristics and the spatial complexity of seismicity, potentially controlled by shared physical mechanisms such as fault roughness, rupture self-similarity, and stress heterogeneity.

Importantly, this study represents the first comprehensive evaluation of the b–Dc relationship across a dense network of seismic zones in Taiwan, providing new empirical support for theoretical scaling laws initially proposed by Aki [1] and Hirata [2]. For instance, in S17A, a strong linear dependence is observed with a slope of 1.76, $R^2 = 0.89$, and $p \approx 4.4\times10^{-5}$, indicating a robust and stable co-evolution of b and Dc, likely governed by consistent rupture and stress-loading conditions. Similarly, zones such as S5B (slope = 2.36, $R^2 = 0.84$), S10 (1.23, $R^2 = 0.72$), and S06 (3.26, $R^2 = 0.82$) exhibit narrow confidence bounds and high explanatory power, reinforcing the notion of strong physical coupling in structurally complex or stress-concentrated regions. In contrast, a subset of zones (e.g., S14B, S15, S17B) exhibits weak or statistically insignificant correlations ($p > 0.05$), which may result from limited b-value variability, small sample sizes, or heterogeneous seismic regimes. In these areas, Dc may be governed more by structural controls or fault geometry than by the magnitude-frequency distribution.

Spatially, the distribution of b–Dc coupling appears to align with tectonic settings. Empirical support for this finding is provided by Wyss et al. [7], who documented a similar b–Dc relationship along the Parkfield segment of the San Andreas Fault. Their work highlighted how creeping and locked segments occupy distinct positions on the b–Dc trend line a pattern that our results echo in Taiwan, where tectonic regimes shift sharply over short distances. Likewise, Bayrak et al. [8] and Solak and Gezgin [22] found that regions in western Anatolia characterized by low b and high Dc values frequently coincide with asperity zones of concentrated stress and heightened seismic hazard. Conversely, high b and high Dc combinations indicated diffuse seismicity under lower stress levels. Based on previous studies, analogous behavior appears in several of our zones (e.g., S06, S09), where elevated Dc-values occur even at moderate b-values, suggesting potential asperity-like stress concentrations. Northern and northeastern zones (S04, S5A, S14A), situated along the subduction interface and back-arc deformation zones, show moderate and consistent coupling. Central zones (S06, S10), located within

the orogenic core along the Central Range, demonstrate extreme slopes and strong co-variation, potentially reflecting elevated strain accumulation and fluid-influenced stress conditions. Southern zones (e.g., S07, S12) show more subdued trends, possibly due to lower strain rates and smoother fault geometries.

From a dynamic perspective, Helmstetter et al. [9], WU et al. [23] and Chen et al. [24] demonstrated that when b > D/2b, microseismicity contributes significantly to stress redistribution and the initiation of subsequent events. The observed slope values offer insights into the physical interpretation of the b–Dc relationship. Slopes between 1 and 2 are consistent with classical scaling relations, where increases in b (indicating higher proportions of small earthquakes) are accompanied by more spatially distributed seismicity (higher Dc). Steeper slopes (>2), as seen in S06 and S5B, may indicate heightened sensitivity of spatial clustering to frequency–magnitude changes, possibly due to localized stress perturbations, fluid overpressure, or rupture complexity. Shallower slopes (<1), such as in S15 and S14B, imply that changes in b-value have less influence on Dc, suggesting decoupled mechanisms or dominant structural constraints.

These findings underscore the potential utility of the b–Dc relationship as a diagnostic tool for stress evolution and rupture dynamics. Given that b-values often decrease prior to major earthquakes and Dc may increase in response to stress concentration, joint monitoring of these parameters could enhance early warning capabilities. In particular, high-sensitivity regions such as S06 may serve as candidate zones for real-time b–Dc-based seismic hazard forecasting.

Figures 6 and 7 illustrate the Kendall and Pearson correlation matrices between the Gutenberg–Richter frequency–magnitude b-value and the correlation fractal dimension (Dc) across all 28 seismic zones.

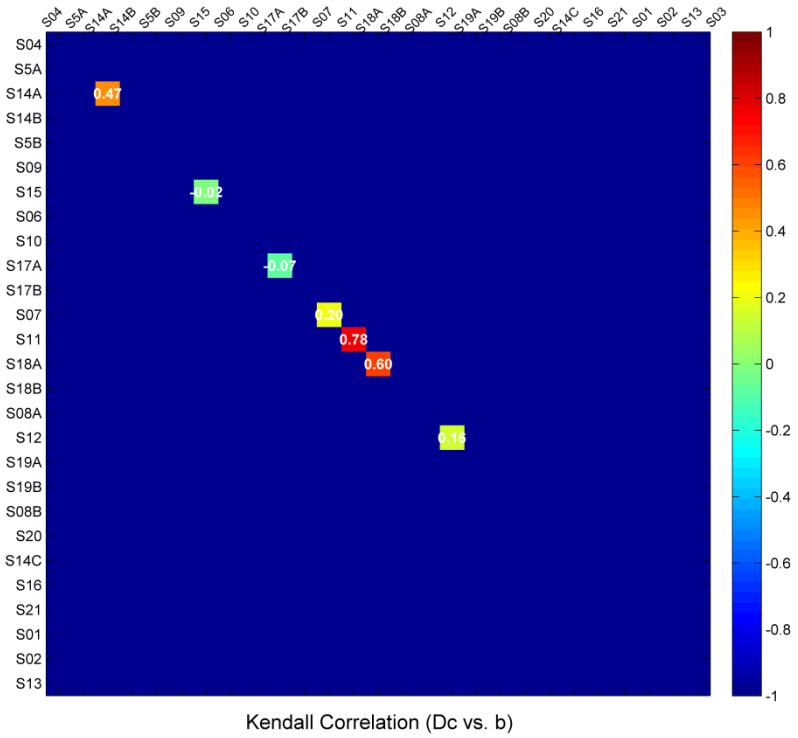

Figure 6.
Kendall correlation coefficients (τ) between the Gutenberg–Richter b-value and the correlation fractal dimension (Dc) across the 28 seismic zones in Taiwan are analyzed. Only statistically significant correlations are displayed, with color coding indicating the strength and direction of the relationship. Positive correlations (e.g., S11, S18A) suggest synchronous evolution of stress state and rupture heterogeneity, whereas weak or negative correlations indicate more complex or decoupled behaviors.

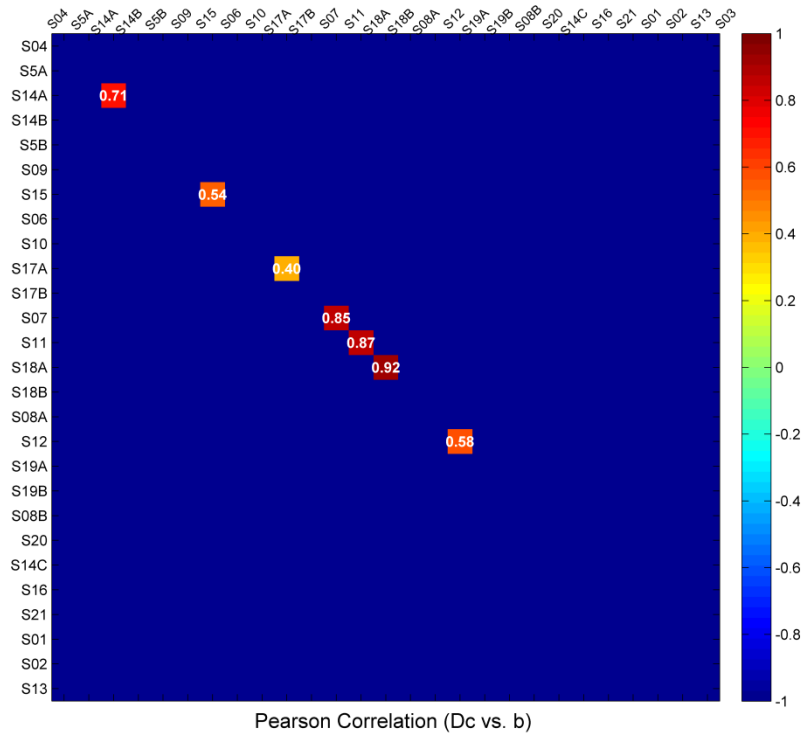

Figure 7.
Pearson correlation coefficients (r) between the Gutenberg–Richter b-value and the correlation fractal dimension (Dc) across the 28 seismic zones in Taiwan. Strong positive linear correlations are observed in several zones (e.g., S11, S18A, S17B), with coefficients exceeding 0.85. These results highlight zones where decreases in b-value (increased stress and proportion of larger earthquakes) coincide with increases in Dc (enhanced spatial heterogeneity), reflecting asperity-driven seismotectonic processes.

The use of both Kendall's τ and Pearson's r provides a complementary assessment of the relationship: while Kendall's τ is more sensitive to the monotonicity of temporal trends, Pearson's r captures the strength of linear dependence. The combined approach ensures that the observed relationships are not artifacts of a particular statistical measure but reflect genuine coupling between the two parameters. The results reveal several zones where b and Dc exhibit strong and consistent positive correlations. In particular, zones S11 and S18A show the highest levels of agreement, with Pearson coefficients exceeding 0.85 and Kendall coefficients greater than 0.60. These findings imply that decreases in b-value, indicating a relative enrichment of large-magnitude events and enhanced differential stress, are simultaneously accompanied by increases in Dc, reflecting more heterogeneous and fragmented rupture patterns. This coupled behavior is consistent with the concept of asperity-dominated rupture processes, where stress accumulation not only promotes the likelihood of larger earthquakes but also drives fault system complexity. Such highly correlated zones may thus represent critical asperity regions that warrant close monitoring as potential precursors of large earthquakes.

Conversely, other zones, such as S15 and S17A, show only weak to moderate correlations (Pearson $r \approx 0.40–0.54$, Kendall $\tau \approx -0.07$ to 0.20). These weaker or even slightly negative correlations suggest that the interplay between seismic energy release and the spatial organization of hypocenters may be less synchronized, potentially due to multi-fault interactions, background seismicity dominance, or transient stress perturbations. In these cases, the relationship between fault stress state and rupture heterogeneity may be more complex and less amenable to simple linear or monotonic descriptions.

Overall, the dual correlation analysis highlights a fundamental finding: while some zones display robust b–Dc coupling indicative of stress-controlled asperities (e.g., S11, S18A), others reflect more diffuse or stochastic regimes. This dichotomy provides new insights into the seismotectonic behavior of Taiwan, suggesting that the combined use of b and Dc as joint indicators may serve as a valuable diagnostic tool in time-dependent seismic hazard assessment. By identifying zones where stress accumulation and fault heterogeneity evolve in tandem, this framework advances the potential for integrating statistical seismology with physical earthquake forecasting models.

4. Conclusion

This study provides the first systematic, island-wide investigation of the statistical coupling between the Gutenberg–Richter b-value and the correlation fractal dimension (Dc) across multiple seismic zones in Taiwan. The results reveal a robust and regionally coherent positive correlation between b and Dc in a majority of zones, with regression slopes predominantly ranging from approximately 1.0 to 2.5, consistent with theoretical predictions and past empirical studies. In several zones, such as S06, S5B, and S17A, the b–Dc relationship is strong, featuring high R^2 values and narrow confidence intervals, indicating a stable, physically meaningful linkage between magnitude distribution and hypocenter spatial complexity.

Complementary correlation analyses using both Kendall's τ and Pearson's r (Figures XX and XX) further highlight the robustness of this relationship. In particular, zones such as S11 and S18A display exceptionally strong positive correlations (Pearson $r > 0.85$, Kendall $\tau > 0.60$), suggesting that decreases in b-value (reflecting stress accumulation and enrichment of larger events) are synchronously accompanied by increases in Dc (indicating rupture heterogeneity and spatial clustering). These zones likely correspond to asperity-dominated fault segments, where stress build-up and structural complexity evolve in tandem. By contrast, zones such as S15 and S17A exhibit weaker or inconsistent correlations, implying that in these regions, the coupling between stress state and seismic clustering is more diffuse, potentially due to multi-fault interactions or transient perturbations.

These findings suggest that the frequency–magnitude characteristics of seismicity (b-value) and the spatial geometry of earthquake occurrence (Dc) are not independent but may be jointly governed by underlying physical processes such as stress heterogeneity, fault zone complexity, and rupture dynamics. Zones with high Dc sensitivity to b-value fluctuations, especially in western and central Taiwan (e.g., S06, S10, S11, S18A), may correspond to asperity-like structures or transitional tectonic domains, where small changes in stress or seismicity patterns produce significant spatial reconfigurations. From a seismotectonic perspective, the observed spatial variations in the b–Dc relationship closely follow regional geological features: moderate coupling is found in subduction interface and arc–backarc transition zones (e.g., S04, S5A), while extreme sensitivities occur in the high-strain belts of central Taiwan, and weaker correlations emerge in relatively stable or geometrically constrained settings (e.g., S15, S14B). This spatial coherence underscores the diagnostic potential of b–Dc coupling as a seismogenic indicator.

Looking ahead, the b–Dc relationship holds promise not only as a fundamental descriptor of seismicity but also as a candidate precursor signal. Given that b-values are known to decrease prior to large earthquakes and Dc may increase with rising stress concentration, a joint monitoring framework that tracks both parameters could offer improved resolution in identifying critical stress conditions. Furthermore, applying this framework in a time-dependent manner using moving windows or machine learning–based models may enable early detection of seismogenic transitions or fault segment reactivation. Future work should expand this approach to incorporate temporal dynamics, cross-validate with geodetic and geologic data (e.g., slip rates, fluid pressure), and explore physical models that can reproduce the observed nonlinear sensitivities. Ultimately, the integration of b–Dc coupling into seismic hazard assessment and early warning systems could enhance the predictive capacity and physical interpretability of earthquake forecasting models in complex tectonic regions like Taiwan.

References

[1] K. Aki, "Maximum likelihood estimate of b in the formula log N= a-bM and its confidence limits," *Bull Earthquake Research Institute, the University of Tokyo,* vol. 43, pp. 237-239, 1965.

[2] T. Hirata, "Fractal dimension of fault systems in Japan: Fractal structure in rock fracture geometry at various scales," *Pure and applied Geophysics,* vol. 131, no. 1, pp. 157-170, 1989. https://doi.org/10.1029/JB094iB06p07507

[3] D. L. Turcotte, *Fractals and chaos in geology and geophysics*. Cambridge: Cambridge University Press, 1997.

[4] C. H. Scholz, "On the stress dependence of the earthquake b value," *Geophysical Research Letters,* vol. 42, no. 5, pp. 1399-1402, 2015. https://doi.org/10.1002/2014GL062863

[5] P. Grassberger and I. Procaccia, "Measuring the strangeness of strange attractors," *Physica D: Nonlinear Phenomena,* vol. 9, no. 1-2, pp. 189-208, 1983. https://doi.org/10.1016/0167-2789(83)90298-1

[6] K. Nanjo and H. Nagahama, "Fractal properties of spatial distributions of aftershocks and active faults," *Chaos, Solitons & Fractals,* vol. 19, no. 2, pp. 387-397, 2004.

[7] M. Wyss, C. G. Sammis, R. M. Nadeau, and S. Wiemer, "Fractal dimension and b-value on creeping and locked patches of the San Andreas fault near Parkfield, California," *Bulletin of the Seismological Society of America,* vol. 94, no. 2, pp. 410-421, 2004.

[8] E. Bayrak, Ş. Yılmaz, and Y. Bayrak, "Temporal and spatial variations of gutenberg-richter parameter and fractal dimension in Western Anatolia, Turkey," *Journal of Asian Earth Sciences,* vol. 138, pp. 1-11, 2017. https://doi.org/10.1016/j.jseaes.2017.01.031

[9] A. Helmstetter, Y. Y. Kagan, and D. D. Jackson, "Importance of small earthquakes for stress transfers and earthquake triggering," *Journal of Geophysical Research: Solid Earth,* vol. 110, no. B5, p. B05S08, 2005. https://doi.org/10.1029/2004JB003286

[10] R. K. Tiwari and H. Paudyal, "Spatial mapping of b-value and fractal dimension prior to November 8, 2022 Doti Earthquake, Nepal," *Plos one,* vol. 18, no. 8, p. e0289673, 2023. https://doi.org/10.1371/journal.pone.0289673

[11] S. M. Ali and K. Abdelrahman, "Analysis of the fractal dimension, b-value, slip ratio, and decay rate of aftershock seismicity following the 6 February 2023 (mw 7.8 and 7.5) türkiye earthquakes," *Fractal and Fractional,* vol. 8, no. 5, p. 252, 2024. https://doi.org/10.3390/fractalfract8050252

[12] A. Firoozfar and B. Ansari, "b-value and fractal dimension variations in Iran," *Earthquake Science,* vol. 32, no. 2, pp. 57-63, 2020. https://doi.org/10.29382/eqs-2019-0057-02

[13] A. Setyawan and B. Sapiie, "Seismicity patterns and aftershock decay analysis in Sumatra," *Natural Hazards and Earth System Sciences Discussions,* 2019.

[14] A. Ghosal, U. Ghosh, and J. Kayal, "A detailed b-value and fractal dimension study of the March 1999 Chamoli earthquake (M s 6.6) aftershock sequence in western Himalaya," *Geomatics, Natural Hazards and Risk,* vol. 3, no. 3, pp. 271-278, 2012. https://doi.org/10.1080/19475705.2011.627380

[15] A. Kumar *et al.*, "The b-value and fractal dimension of local seismicity around Koyna Dam (India)," *Earthquake Science,* vol. 26, no. 2, pp. 99-105, 2013. https://doi.org/10.1007/s11589-013-0008-1

[16] P. Mandal *et al.*, "Three-dimensional b-value and fractal dimension mapping of the Uttarakhand Himalayan region," *Journal of the Geological Society of India,* vol. 98, no. 10, pp. 1365-1379, 2022. https://doi.org/10.1007/s12594-022-2184-x

[17] P. Mandal *et al.*, "Assessment of the earthquake hazard in the Ladakh and neighbouring Himalayan region (India) utilizing three-dimensional modelling of b-value and fractal (correlation) dimensions," *Geoenvironmental Disasters*, vol. 12, no. 1, p. 8, 2025. https://doi.org/10.1186/s40677-025-00314-y

[18] J. Woessner and S. Wiemer, "Assessing the quality of earthquake catalogues: Estimating the magnitude of completeness and its uncertainty," *Bulletin of the Seismological Society of America*, vol. 95, no. 2, pp. 684-698, 2005.

[19] S. Wiemer and M. Wyss, "Mapping spatial variability of the frequency-magnitude distribution of earthquakes," *Advanced Geophysics*, vol. 45, pp. 259–302, 2022. https://doi.org/10.1016/S0065-2687(02)80007-3

[20] C.-T. Cheng, P.-S. Hsieh, P.-S. Lin, Y.-T. Yen, and C.-H. Chan, *Probability seismic hazard mapping of Taiwan*. Berlin, Heidelberg: Springer, 2015.

[21] J. Gardner and L. Knopoff, "Is the sequence of earthquakes in Southern California, with aftershocks removed, Poissonian?," *Bulletin of the Seismological Society of America*, vol. 64, no. 5, pp. 1363-1367, 1974. https://doi.org/10.1785/BSSA0640051363

[22] H. İ. Solak and C. Gezgin, "Seismic hazard evaluation and strain dynamics in the simav fault zone: A comprehensive analysis of earthquake recurrence and energy release patterns," *Applied Sciences*, vol. 15, no. 6, p. 3039, 2025. https://doi.org/10.3390/app15063039

[23] H.-Y. WU, L. Hong-Fu, X. Wei-Jin, and W. Xia, "Fractal dimension and b value of the aftershock sequence of the 2008 MS 8.0 Wenchuan earthquake," *Natural Hazards*, vol. 88, no. 1, pp. 315-325, 2017. https://doi.org/10.1007/s11069-017-2866-7

[24] C.-C. Chen, W.-C. Wang, Y.-F. Chang, Y.-M. Wu, and Y.-H. Lee, "A correlation between the b-value and the fractal dimension from the aftershock sequence of the 1999 Chi-Chi, Taiwan, earthquake," *Geophysical Journal International*, vol. 167, no. 3, pp. 1215-1219, 2006. https://doi.org/10.1111/j.1365-246X.2006.03230.x